The high resolution infrared spectrum of ethylene in the 1800 cm-1 to 2350 cm-1 spectral region

W.J. Lafferty, Jean Marie Flaud, Fridolin Kwabia

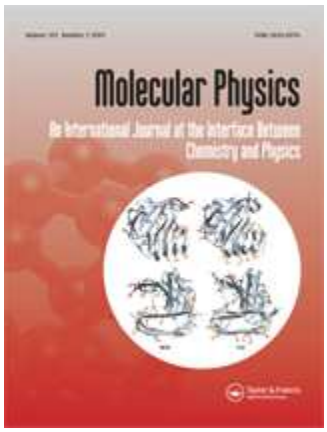

The high resolution infrared spectrum of ethylene in the 1800 cm-1 to 2350 cm-1 spectral region

Journal:	*Molecular Physics*
Manuscript ID:	TMPH-2010-0385.R1
Manuscript Type:	Full Paper
Date Submitted by the Author:	09-Mar-2011
Complete List of Authors:	Lafferty, W.J.; NIST FLAUD, Jean Marie; LISA KWABIA, Fridolin; LISA
Keywords:	Infrared, Ethylene, Rovibrational interactions, line positions and intensities
Note: The following files were submitted by the author for peer review, but cannot be converted to PDF. You must view these files (e.g. movies) online.	
TMPH-2010-0385.R1.zip	

The high resolution infrared spectrum of ethylene in the 1800 cm^{-1} to 2350 cm^{-1} spectral region

W.J. Lafferty

Optical Technology Division, National Institute of Standards and Technology, Gaithersburg, MD 20899-8440, USA

and

J.-M. Flaud and F. Kwabia Tchana,

Laboratoire Interuniversitaire des Systèmes Atmosphériques (LISA), UMR CNRS 7583, Universités Paris Est Créteil et Paris Diderot, Institut Pierre Simon Laplace, 61 Avenue du Général de Gaulle, 94010 Créteil Cedex, France

Abstract

Fourier transform spectra of ethylene (C_2H_4) have been recorded in the 1800 cm^{-1} to 2350 cm^{-1} (4.3 μm to 5.6 μm) spectral region using a Bruker IFS125HR spectrometer at a resolution of 0.004 cm^{-1} leading to the observation of six vibrational bands, $\nu_7 + \nu_8$, $\nu_4 + \nu_8$, $\nu_6 + \nu_{10}$, $\nu_6 + \nu_7$, $\nu_4 + \nu_6$ and $\nu_3 + \nu_{10}$. The corresponding upper state ro-vibrational levels were fit using a Hamiltonian matrix accounting for numerous interactions. A satisfactory fit could be obtained using a polyad of nine interacting states {$8^1 10^1$, $7^1 8^1$, $4^1 8^1$, $8^1 12^1$, $6^1 10^1$, $6^1 7^1$, $4^1 6^1$, $3^1 10^1$, $3^1 7^1$} among which three ($8^1 10^1$, $8^1 12^1$ and $3^1 7^1$) are unobserved dark states. As a result a much more accurate and extended set of Hamiltonian constants were obtained than previously derived. The following band centers were determined: $\nu_0(\nu_7 + \nu_8)$ = 1888.9783(20) cm^{-1}, $\nu_0(\nu_4 + \nu_8)$ = 1958.2850(20) cm^{-1}, $\nu_0(\nu_6 + \nu_{10})$ = 2047.7589(20) cm^{-1}, $\nu_0(\nu_6 + \nu_7)$ = 2178.011(60) cm^{-1}, $\nu_0(\nu_4 + \nu_6)$ = 2252.8026(24) cm^{-1} and $\nu_0(\nu_3 + \nu_{10})$ = 2171.2397(20) cm^{-1}. Finally, a synthetic spectrum which could be useful for ethylene detection in planetary atmospheres was generated.

1. Introduction

Ethylene (C_2H_4) is observed in the terrestrial atmosphere as a tropospheric pollutant produced by automobiles, forest fires and plant life [1]. In the atmosphere, photochemical reactions with molecular oxygen, the hydroxyl radical, and ozone produce formaldehyde, nitrous oxide, and formic acid [2]. C_2H_4 is also detected in the atmospheres of the outer solar system bodies including Jupiter [3], Saturn [4], and Neptune and Titan [5-7]. In these atmospheres it is a by-product of methane photochemistry.

Spectroscopically, ethylene is an asymmetric top molecule which has been the subject of a number of studies concerning either the normal isotopic species $^{12}C_2H_4$ or the $^{13}C^{12}CH_4$ istopomer. However these studies dealt mainly with the 10 μm region bands, where the strongest band is the C-type ν_7 band [8-10 and ref. therein, 11-12]. Nevertheless, prior to this work, only small portions of the 4.3 μm to 5.6 μm region, corresponding to the $\nu_7 + \nu_8$ and $\nu_4 + \nu_8$ bands have been analyzed [13-15]. More recently, three high-resolution infrared and Raman spectra of $^{12}C_2H_4$ were recorded and analyzed: the ν_{12} band near 1450 cm^{-1} [16], the $2\nu_{10}$ overtone symmetric motion located around 1664 cm^{-1} [17] and the C-H stretching vibrations in the 3000 and 6000 cm^{-1} regions [18].

In this paper, we present an extensive analysis of the 4.3 μm to 5.6 μm region and have assigned six vibrational bands, $\nu_7 + \nu_8$, $\nu_4 + \nu_8$, $\nu_6 + \nu_{10}$, $\nu_6 + \nu_7$, $\nu_4 + \nu_6$ and $\nu_3 + \nu_{10}$. This was carried out using two high-resolution Fourier transform spectra recorded at two different pressures in order to obtain precise line position for both the weak as well as the strong bands. The upper state ro-vibrational levels were fit using a Hamiltonian (written in the I^r (x = b, z = a, y = c) representation) model taking into account the numerous interactions affecting them. We note that it was necessary to consider interactions not only between levels of the observed states but also with levels of unobserved dark states. In this way a satisfactory fit was performed leading to Hamiltonian constants much more accurate than obtained in previous studies even though the accuracy of the fits was slightly worse than the experimental uncertainties. The ethylene (C_2H_4) molecule possesses D_{2h} symmetry and its structure as well as its symmetry properties and nuclear spin statistical weights are illustrated in Figure 1.

2. Experimental details

The high-resolution absorption spectra of ethylene were recorded with the Bruker IFS125HR Fourier transform spectrometer[1] (an upgraded version of the IFS120HR) located at the LISA facility, in Créteil. A KBr beamsplitter, Globar source (Silicon Carbide, SiC) and a liquid nitrogen-cooled Indium Antimonide (InSb) detector were employed for these experiments. The optical path of the spectrometer was continuously evacuated to below 6.7 Pa (0.05 Torr) for the duration of all spectral measurements. Spectra were recorded with an aperture diameter of 1.3 mm, 40 kHz scanner frequency, and a maximum optical path difference (d_{MOPD}) of 225 cm. According to the Bruker definition (Resolution = $0.9/d_{MOPD}$) this corresponds to a resolution of 0.004 cm^{-1}. This resolution is limited by the Doppler widths which is equal to 0.0042 cm^{-1} at 1800 cm^{-1}.

The White-type multipass absorption cell, made of pyrex glass and equipped with CsBr windows, was connected to the Fourier transform spectrometer with a dedicated optical interface (six mirrors) inside the back sample compartment of the Bruker spectrometer. Its base length is 0.80 m, and, for the experiment described here, an optical path of 19.2 m was used. The ethylene sample was purchased from Sigma Aldrich. The chemical purity of ethylene was specified to 99.99 % and was used without further purification. The following procedure was used for measurements: First a background spectrum was collected while the cell was being continuously evacuated. Next a calibration spectrum was recorded with carbonyl sulfide (high purity sample at low pressure). The absorption cell was then evacuated, and flushed several times with dry nitrogen until the base pressure of the cell 1.3 x 10^{-3} Pa (10^{-5} Torr) was achieved. Two ethylene

[1] Certain commercial equipment instruments or materials are identified in this paper to adequately specify the experimental procedure. Such identification does not imply recommendation or endorsement by the National Institute of Standards and Technology nor does it imply that the materials or equipment identified are necessarily the best available for the purpose.

spectra were then recorded with 16.41 (1) Pa (0.1231 (1) Torr) and 65.97 (8) Pa (0.4948 (6) Torr). Sample pressure in the cell was measured using a calibrated MKS Baratron capacitance manometer (266 Pa full scale) which has a stated uncertainty of 0.12 % of full scale, according to the manufacturer. The spectra were recorded at a stabilized room temperature of 22°C. Both spectra were ratioed against the empty cell, single-channel background spectrum which was taken at a resolution of 0.512 cm^{-1}, in order to ensure the best possible signal-to-noise in the ratioed spectra. The spectra were the result of the co-addition of 550 interferograms. For the Fourier transform a Mertz-phase correction, 0.5 cm^{-1} phase resolution and boxcar apodization function were applied to the averaged interferograms. The spectra were calibrated using OCS lines from HITRAN08 [19] resulting in an accuracy of 0.00012 cm^{-1} (RMS) for well isolated lines.

Fig. 2 gives an overview of the ethylene spectra showing the high signal-to-noise ratios which were obtained. The distinctive shape of the two A-type $\nu_7 + \nu_8$ (around 1889 cm^{-1}) and $\nu_6 + \nu_{10}$ (around 2047 cm^{-1}) bands with their narrow Q-branches are clearly visible.

3. Assignments and results.

The line assignment process proved to be very difficult since a number of bands fall in the 4.3 μm to 5.6 μm region and the number of ro-vibration interactions is high. This includes interactions not only between the levels of the observed states but also with dark state levels. We initially started the assignment process dealing with the strong $\nu_7 + \nu_8$ band, but, as pointed out in refs. [13-15], it soon became obvious that its transitions are strongly perturbed by $\nu_4 + \nu_8$ transitions through a C-type Coriolis interaction via the $\xi^a_{7,10}$ and $\xi^b_{4,10}$ Coriolis interaction terms [10]. In addition, we observed other interactions with the $8^1 10^1$ and $8^1 12^1$ energy levels which correspond with what has been observed at 10 μm where the polyad of interacting states $\{10^1, 8^1, 7^1, 12^1\}$ was considered. Using a Hamiltonian matrix taking into account the necessary interaction terms, it was possible to assign many lines of $\nu_7 + \nu_8$ and $\nu_4 + \nu_8$. During this process, it became very clear that the ro-vibrational levels of $4^1 8^1$ and $7^1 8^1$ are also perturbed by nearby rotational levels from bands belonging to other polyads [13]. We then started to assign transitions belonging to these other bands: $\nu_6 + \nu_{10}$, $\nu_6 + \nu_7$, $\nu_4 + \nu_6$ and $\nu_3 + \nu_{10}$. This was done with the aid of

a Hamiltonian matrix including the observed states as well as some resonating dark states (Fig. 3, Table 1). The assignment process was repeated until it was no longer possible to locate and assign new lines with confidence. The range of the assigned energy levels for each band is given in Table 2. Even if the experimental accuracy (ca. 0.0002 cm^{-1} for isolated lines) is not reached, given the fact that there are numerous resonances and that it was necessary to include dark states in the calculations, we feel that the fit is rather satisfactory, since the standard deviation is 0.002 cm^{-1} with a maximum difference of 0.016 cm^{-1} (see Table 2 for further details). The corresponding Hamiltonian constants can be found in Table 3.

4. Intensity measurements.

The intensity of a line is given in $cm^{-1}/(molecule.cm^{-2})$ by [20, 21]:

$$k_{\tilde{\nu}}^{N} = \frac{8\pi^3\tilde{\nu}}{4\pi\varepsilon_0 3hcZ(T)} g_n \left(1-\exp\left(-\frac{hc\tilde{\nu}}{kT}\right)\right)\exp\left(-\frac{hcE_A}{kT}\right)R_A^B \qquad (1)$$

where A and B are respectively the lower and upper levels of the transition, $\tilde{\nu} = (E_B - E_A)/hc$ is the wavenumber of the transition, Z(T) is the total partition function depending on the temperature (we used Z(296K) = 44165.84 [19]) and g_n is the nuclear spin statistical weight. Finally, R_A^B is the square of the matrix element of the transformed transition moment operator μ'_Z.

μ'_Z is expanded as:

$$\mu'_Z = \sum_{v'\in B'} |0\rangle\, {}^{v}\mu_Z \langle v'| \qquad (2)$$

where v' belongs to the upper B' polyad of interacting states.

Then depending on the band symmetry the transition moment operators can be written [20]:

$$^{v}\mu_Z = \varphi_x \; ^{v}\mu_x^1 + \{\varphi_z, iJ_y\} \; ^{v}\mu_x^5 + \text{...??????????? for a B-type band}$$

$$^{v}\mu_Z = i\varphi_y \; ^{v}\mu_y^1 + \{\varphi_z, J_x\} \; ^{v}\mu_y^5 + \text{.... for a C-type band ???} \quad (3)$$

$$^{v}\mu_Z = \varphi_z \; ^{v}\mu_z^1 + \frac{1}{2}\left(\{\varphi_x, iJ_y\} - \{i\varphi_y, J_x\}\right) \; ^{v}\mu_z^4 + \text{.... for an A-type band}$$

where φ_x, φ_y and φ_z stand for the direction cosines Φ_{Zx}, Φ_{Zy} and Φ_{Zz} respectively.

The transition moment constants (see Eqs.(3)) are determined through a least squares fit of the experimental line intensities. Using the low pressure spectrum, 264 line intensities were measured (39, 94, 49, 11, 29 and 42 lines for $\nu_7 + \nu_8$, $\nu_4 + \nu_8$, $\nu_6 + \nu_{10}$, $\nu_6 + \nu_7$, $\nu_4 + \nu_6$ and $\nu_3 + \nu_{10}$ respectively.) and fit using Eq.(1-3). The fit is satisfactory since 71% of the experimental line intensities were calculated to within 7% with a maximum discrepancy of 28%. Finally the absolute intensities were calibrated using the PNL (Pacific Northwest Laboratory) measurements [22]. In this way it was possible to determine the transition moment parameters gathered in Table 4. These parameters together with the wavefunctions derived from the diagonalization of the Hamiltonian matrix were used to generate a list of line positions and intensities (Cut off of 1.5 X 10^{-24} cm^{-1}/(molecule.cm^{-2}) at 296K)[2]. Fig. 2 presents a simulation of the whole spectral region performed using this line list: one notes the very good agreement between the observed and calculated spectra.

5. Discussion

As found previously [13] as well as observed in this work, a large number of resonances perturb the ro-vibrational levels of the polyad of interacting states {$8^1 10^1$, $7^1 8^1$, $4^1 8^1$, $8^1 12^1$, $6^1 10^1$, $6^1 7^1$, $4^1 6^1$, $3^1 10^1$, $3^1 7^1$}. We describe them here in some detail in order to demonstrate the resonance scheme used to build the Hamiltonian matrix.

[2] The list of line positions and intensities is available upon request to J.-M. Flaud or W. J. Lafferty.

Field Code Changed

Formatted: Indent: First line: 0 pt

Deleted: ¶

Formatted: Font: 12 pt, Not Superscript/ Subscript

Formatted: Font: Times New Roman, 12 pt, Not Superscript/ Subscript

Formatted: English (U.S.), Not Superscript/ Subscript

Once the Hamiltonian matrix has been diagonalized, the wave function of a ro-vibrational level can been determined as:

$$\left|v_i^{'}, J'K'_aK'_c\right\rangle = \sum_{v'\in P'}\sum_{K',\gamma'} C_{K'\gamma'}^{v'}\left|v'\right\rangle\left|J'K'\gamma'\right\rangle \qquad (2)$$

where the $|JK\gamma>$ are the classical Wang-type functions:

$$\left|JK\gamma\right\rangle = \frac{1}{\sqrt{2}}\left(\left|JK\right\rangle + \gamma\left|J-K\right\rangle\right) \text{ (for } K\neq 0,\ \gamma=\pm 1) \qquad (3)$$

$$\left|JK=0\gamma=+1\right\rangle = \left|J0\right\rangle$$

and where P' is the polyad of interacting upper states {$8^1 10^1$, $7^1 8^1$, $4^1 8^1$, $8^1 12^1$, $6^1 10^1$, $6^1 7^1$, $4^1 6^1$, $3^1 10^1$, $3^1 7^1$}. Then the mixing coefficients of the ro-vibrational level $|v_i' J' K'_a K'_c>$ onto the state v' can be defined as $\sum_{K'}\left|C_{K'}^{v'}\right|^2 \times 100$ where the $C_{K'}^{v'}$ are the coefficients appearing in Eq.(2). Fig. 4 presents the mixing coefficients of the $\left|7^1 8^1 JK_a = 8K_c\right\rangle$ and $\left|6^1 7^1 JK_a = 8K_c\right\rangle$ levels onto the $4^1 8^1$ and the $4^1 6^1$ states. While the mixing coefficients of both level series vary smoothly, differences are observed even if the mechanism is identical, i.e. a C-type Coriolis interaction. In particular the crossing of levels happens at different values: J = 9 and J = 12 for $7^1 8^1$ and $6^1 7^1$ respectively. Such resonances are analogous to those observed at 10 μm between the levels of 7^1 and 4^1. On the other hand, we have also observed very localized resonances linking ro-vibrational levels belonging to different polyads of interacting states. For example, the $8_{0\,8}$ level of the $6^1 7^1$ state which gives rise to the forbidden band $\nu_6 + \nu_7$ (A_u symmetry species, Fig. 1) is observed only because it resonates (mixing coefficient of 18%) with the $8_{1\,7}$ level of $3^1 10^1$. In fact, all the transitions involving $8_{0\,8}$ borrow their intensities from those involving $8_{1\,7}$. Fig. 5 presents a portion of the spectrum where the forbidden transition $8_{0\,8}$ - $9_{2\,8}$ of $\nu_6 + \nu_7$ is clearly observable together with the allowed transition 8_{17} - $9_{2\,8}$ of $\nu_3 + \nu_{10}$.

As far as the intensities are concerned we estimated an accuracy of about 5%. Figures 5, 6 and 7 show comparisons of the observed and calculated spectra. The good agreement between observation and simulation demonstrates the quality of the analysis and the fitting. Of particular interest is Fig. 6 where one can see on both sides of the central part of the Q-branch region of

Deleted: as

$\nu_7 + \nu_8$ series of lines concerning the Ka = 8 (Ka = 7) transitions of $\nu_7 + \nu_8$ ($\nu_4 + \nu_8$). Such a behavior is due to the interactions between the corresponding upper levels (see the mixing coefficients in Fig. 4). Finally Fig.8 presents the band intensities derived from the calculations. One can see that the $\nu_3 + \nu_7$ and $\nu_8 + \nu_{12}$ bands are, as discussed previously, very weak.

Deleted: Conclusion

6. Summary.

Using high-resolution Fourier transform spectra an extensive analysis of the 1800 cm^{-1} to 2350 cm^{-1} spectrum of ethylene ($^{12}C_2H_4$) has been performed. The upper state energy levels have been fit to within 2 x 10^{-3} cm^{-1} using a Hamiltonian matrix which takes into account the numerous interaction terms coupling the interacting states {$8^1 10^1$, $7^1 8^1$, $4^1 8^1$, $8^1 12^1$, $6^1 10^1$, $6^1 7^1$, $4^1 6^1$, $3^1 10^1$, $3^1 7^1$}. In this way, accurate band centers, rotational, centrifugal distortion and coupling constants have been determined. Also individual line intensities as well as total band intensities have been measured and fit satisfactorily, and an accurate list of line positions and intensities has been generated.

Acknowledgements

The portion of this work which was carried out at the Optical Technology of NIST was supported by the Upper Atmospheric Research Program of NASA. One of authors (JMF) thanks the Optical Technology Division for support during a stay at NIST.

References

[1] F.B. Abeles, H.E. Heggestad, J. Air Pollut. Control Assoc. 23 (1973) 517-521.

[2] H. Niki, P.D. Maker, C.M. Savage, L.P. Breitenbach, J. Phys. Chem. 82 (1978) 135-137.

[3] T. Kostiuk, F. Espenak, M.J. Mumma, Infrared Phys. 29 (1989) 199-204.

[4] T. Encrenaz, M. Combes, Y. Zeau, L. Vapillon, J. Berenze, Astron Astrophys 42 (1975) 355-356.

[5] R. Hanel, B. Conrath, F.M. Flaser, V. Kunde, W. Maguire, J. Pearl, J. Pirraglia, R. Samuelson, et al., Science 212 (1981) 192-200.

[6] R. Hanel, B. Conrath, F.M. Flaser, V. Kunde, W. Maguire, J. Pearl, et al., Science 215 (1981) 544-548.

[7] W. Maguire, R. Hanel, D.E. Jennings, V.G. Kunde, R.E. Samuelson, Nature 292 (1981) 683-686.

[8] E.Rusinek, H. Fichoux, M. Khelkhal, F. Herlemont, J. Legrand, A. Fayt, J. Mol. Spectrosc. 189 (1998) 64-73.

[9] J. Legrand, M. Aziz, F. Herlemont, A. Fayt, J. Mol. Spectrosc. 139 (1995) 13-21.

[10] I. Cauuet, J. Walrand, G. Blanquet, A. Valentin, L. Henry, Ch. Lambeau, M. De Vleeschouver, A. Fayt, J. Mol. Spectrosc. 139 (1990) 191-214.

[11] J.-M. Flaud, W.J. Lafferty, R. Sams, V. Malathy Devi, J. Mol. Spectrosc. 259 (2010) 39-45.

[12] R. L. Tan, G. B. Breton, J. Mol. Spectrosc. 261 (2010) 63-67.

[13] D. Van Lerberghe, A. Fayt, Mol. Phys. 31 (1976) 1875-1886.

[14] Ch. Lambeau, M. De Vleeschouver, D. Van Lerberghe, A. Fayt, J. P. Kupfer, H. P. Oascher, G. Haefele, Mol. Phys. 46 (1982) 981-990.

[15] D.Hurtmans, A. Rizopoulos, M. Herman, L.M.S. Hassan, A. Perrin, Mol. Phys. 99 (2001) 455-461.

[16] M. Rotger, V. Boudon, J. Vander Auwera, Journal of Quantitative Spectroscopy and Radiative Transfer, 109 (2008) 952-962.

[17] M. Lorono, D. Bermojo, M. Rotger, V. Boudon, J. Raman Spectrosc. 40 (2009) 1065-1071.

[18] M.A. Lorono Gonzalez, V. Boudon, M. Loëte, V. Boudon, et al., Journal of Quantitative Spectroscopy and Radiative Transfer, 111 (2010) 2265-2278.

[19] L.S. Rothman, I.E. Gordon, A. Barbe, D.Chris Benner, P.F. Bernath, M. Birk, V. Boudon, L.R. Brown, A. Campargue, J.-P. Champion, K. Chance, L.H. Coudert, V. Dana, V.M. Devi, S. Fally, J.-M. Flaud, R.R. Gamache, A. Goldman, D. Jacquemart, I. Kleiner, et al., The HITRAN 2008 molecular spectroscopic database, Journal of Quantitative Spectroscopy and Radiative Transfer, 110 (2009) 533-572.

[20] J.-M. Flaud, C. Camy-Peyret, R.A. Toth, Water Vapour Line Parameters from Microwave to Medium Infrared, Pergamon press, Oxford, 1981.

[21] C. Camy-Peyret, J.-M. Flaud, Vibration-rotation dipole moment operator for asymmetric rotors, in: K. Narahari Rao (Ed.), Molecular Spectroscopy Modern Research, vol. 3, Academic Press, New York, 1985, pp. 69–110.

[22] , S. W. Sharpe, T. J. Johnson, R. L. Sams, P. M. Chu, G. C. Rhoderick, P. A. Johnson, Appl. Spectrosc. 58 (2004) 1452-1461.

Captions to figures:

Fig. 1. Structure and symmetry properties of the ethylene molecule.

Fig . 2. Overview of the ethylene spectrum studied in this work. The distinctive shape of the two A-type bands $\nu_7 + \nu_8$ and $\nu_6 + \nu_{10}$ with their narrow Q-branches are clearly recognizable. Upper trace: observed spectrum recorded with a resolution of 0.004 cm^{-1} and an optical path length of 19.2 m, at a C_2H_4 pressure of 16.41 (1) Pa (0.1231 (1) Torr) and a stabilized room temperature of 22 °C. Lower trace: synthetic spectrum, calculated at the same experimental conditions using the line list generated in this work. The observed and synthetic spectra are in absorbance ($-\ln(I/I_0)$) and shifted vertically for clarity.

Fig. 3 Resonating scheme of the ro-vibrational levels of ethylene in the 1700 cm^{-1} to 2400 cm^{-1} region.

Fig. 4. Mixing coefficients of the $K_a = 8$ rotational levels of the $7^1 8^1$, $6^1 7^1$ states onto the $4^1 8^1$, $4^1 6^1$ states respectively.

Fig. 5. A transition of the forbidden $\nu_6 + \nu_7$ band. This transition appears only because of borrowed intensity from the permitted $\nu_3 + \nu_{10}$ line. Upper trace: observed spectrum recorded with a resolution of 0.004 cm^{-1} and an optical path length of 19.2 m, at a C_2H_4 pressure of 16.41 (1) Pa (0.1231 (1) Torr) and a stabilized room temperature of 22 °C. Lower trace: synthetic spectrum, calculated at the same experimental conditions using the line list generated in this work. The observed and synthetic spectra are in absorbance ($-\ln(I/I_0)$) and shifted vertically for clarity.

Fig. 6. Q-branch area of the $\nu_7 + \nu_8$ band. Because of the strong resonance (Fig. 4) the K = 8 line of $\nu_7 + \nu_8$ and the K = 7 perturbation induced transitions of $\nu_4 + \nu_8$ are degraded in opposite directions. Upper trace: observed spectrum recorded with a resolution of 0.004 cm^{-1} and an optical path length of 19.2 m, at a C_2H_4 pressure of 16.41 (1) Pa (0.1231 (1) Torr) and a stabilized room temperature of 22 °C. Lower trace: synthetic spectrum, calculated at the same experimental conditions using the line list generated in this work. The observed and synthetic spectra are in absorbance ($-\ln(I/I_0)$) and shifted vertically for clarity.

Fig. 7. Q-branches of the weak C-type band $\nu_4 + \nu_6$. Upper trace: observed spectrum recorded with a resolution of 0.004 cm^{-1} and an optical path length of 19.2 m, at a C_2H_4 pressure of 16.41 (1) Pa (0.1231 (1) Torr) and a stabilized room temperature of 22 °C. Lower trace: synthetic spectrum, calculated at the same experimental conditions using the line list generated in this work. The observed and synthetic spectra are in absorbance ($-\ln(I/I_0)$) and shifted vertically for clarity.

Structure of the ^{12}C ^{12}C ethylene molecule

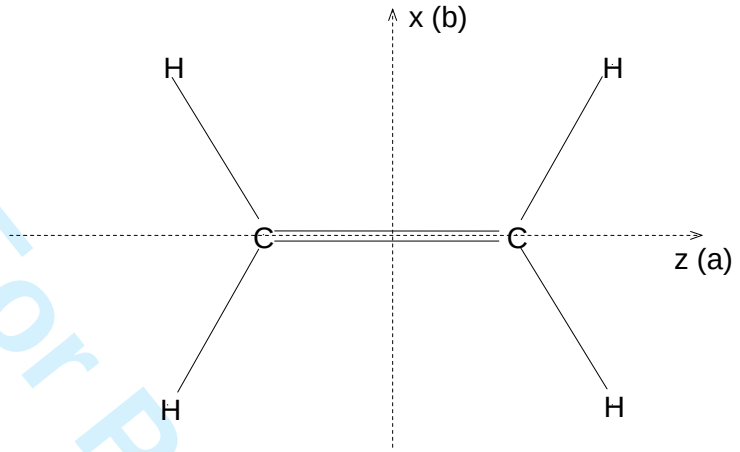

D_{2h} group character table

	I	C_{2x}	C_{2y}	C_{2z}	i	σ_{xz}	σ_{yz}	σ_{xy}	Polar vector	Axial vector	Vibrations
A_g	1	1	1	1	1	1	1	1			ν_1,ν_2,ν_3
A_u	1	1	1	1	-1	-1	-1	-1			ν_4
B_{1g}	1	-1	1	-1	1	1	-1	-1		R_y	ν_5,ν_6
B_{1u}	1	-1	1	-1	-1	-1	1	1	T_y		ν_7
B_{2g}	1	1	-1	-1	1	-1	1	-1		R_x	ν_8
B_{2u}	1	1	-1	-1	-1	1	-1	1	T_x		ν_9,ν_{10}
B_{3g}	1	-1	-1	1	1	-1	-1	1		R_z	
B_{3u}	1	-1	-1	1	-1	1	1	-1	T_z		ν_{11},ν_{12}

Nuclear spin statistical weights for the ground state rotational levels

K_a	K_c	Weight
Even	Even	7
Even	Odd	3
Odd	Even	3
Odd	Odd	3

Fig. 1

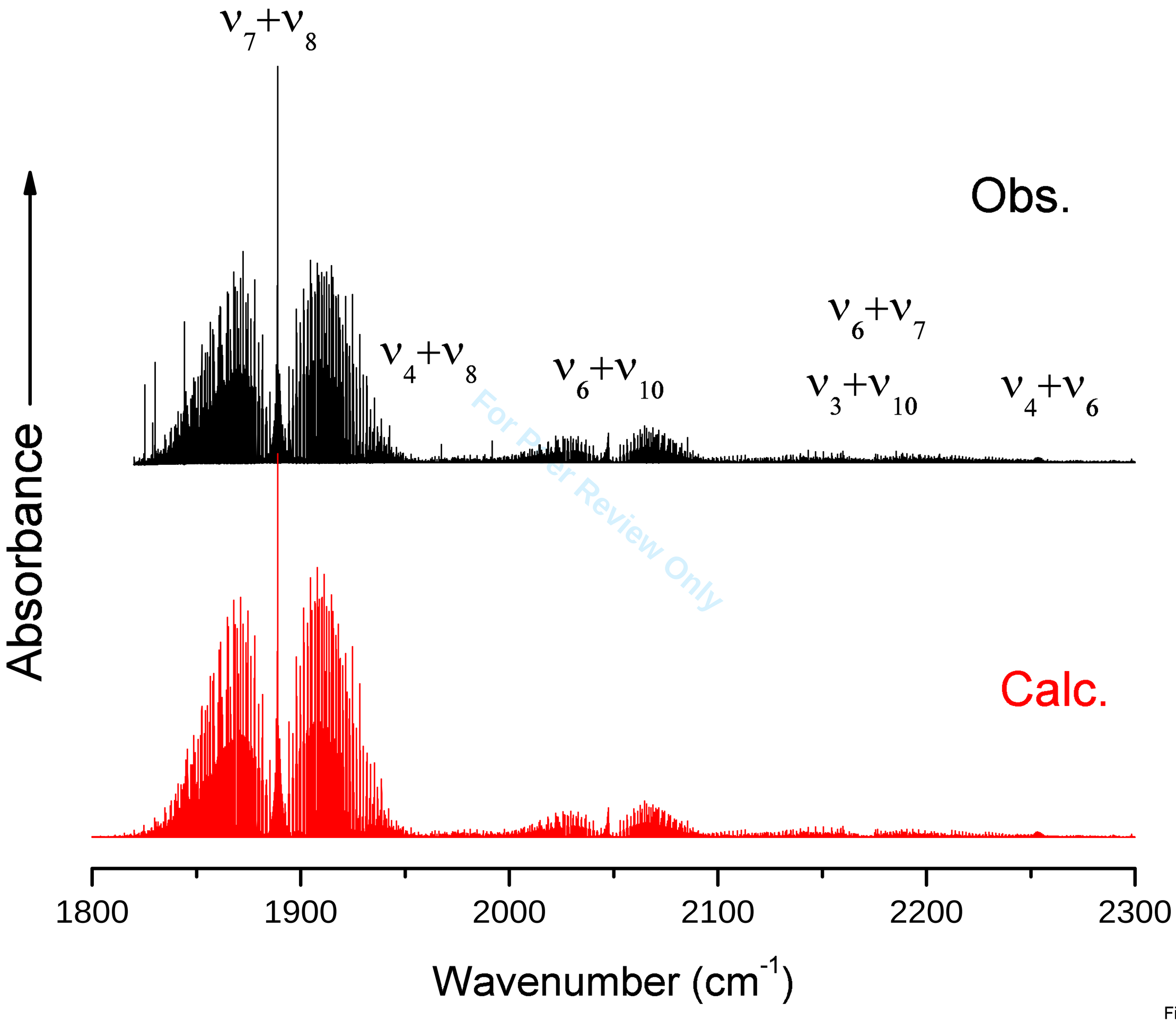

Fig. 2

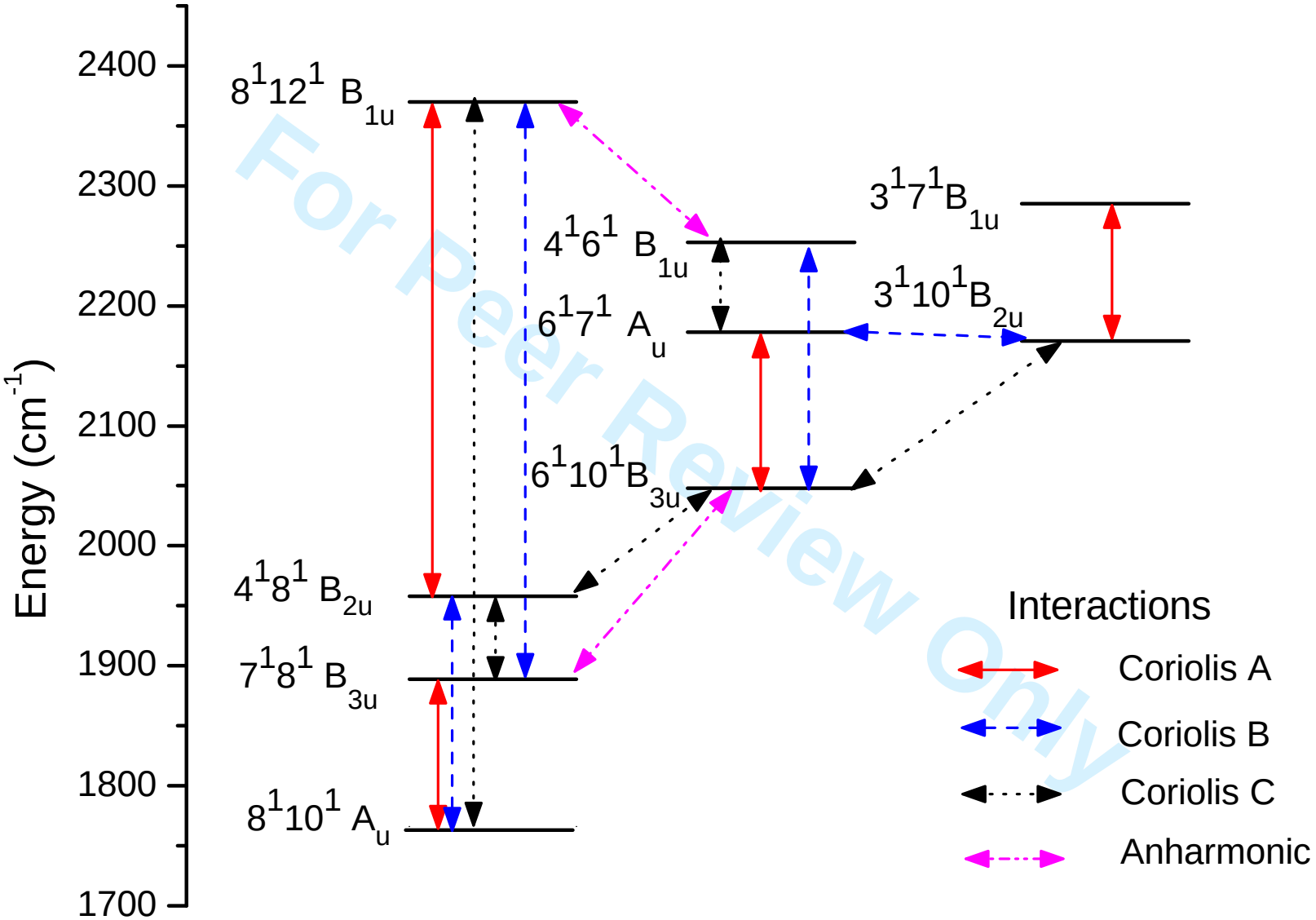

Fig. 3

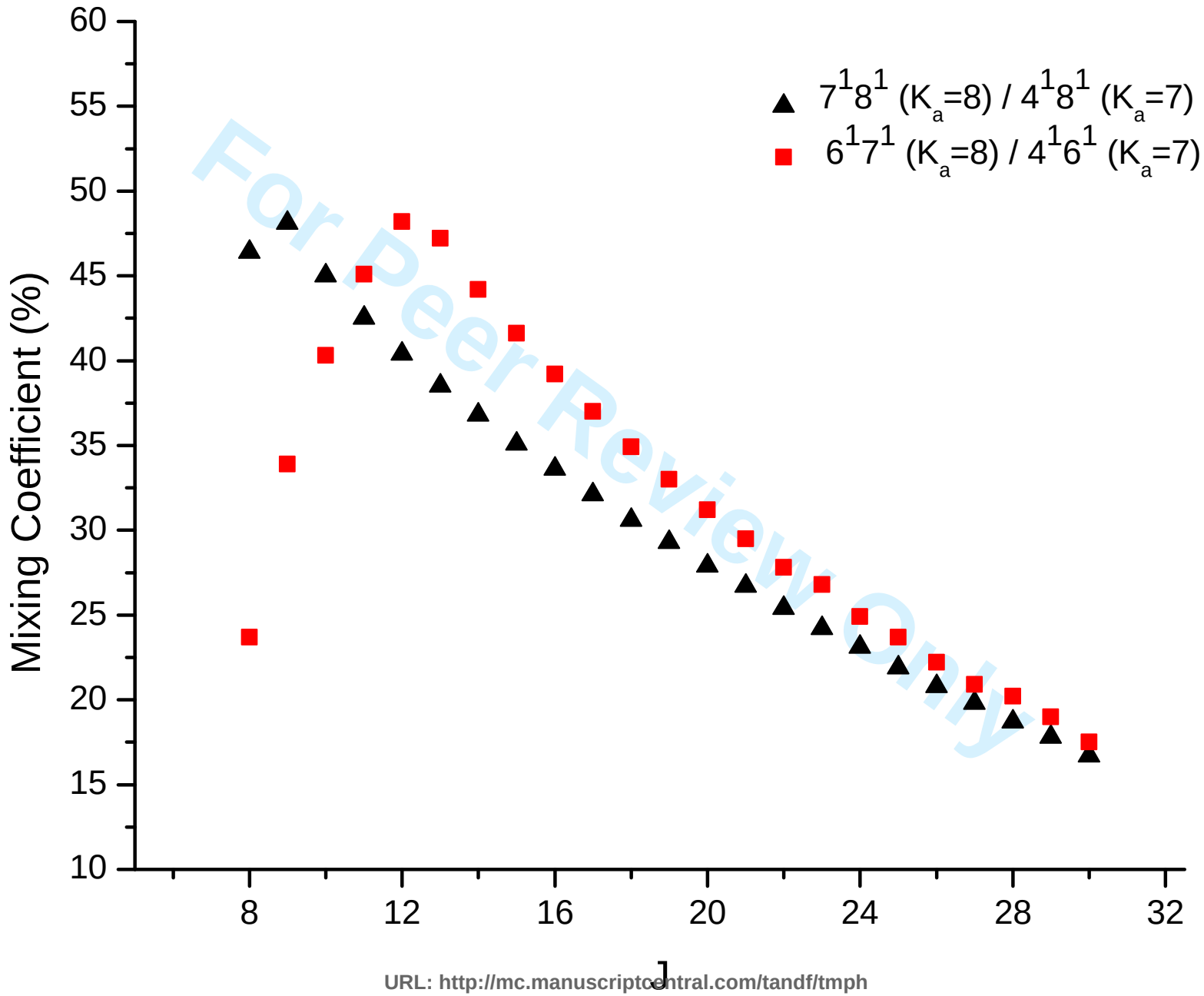

Fig. 4

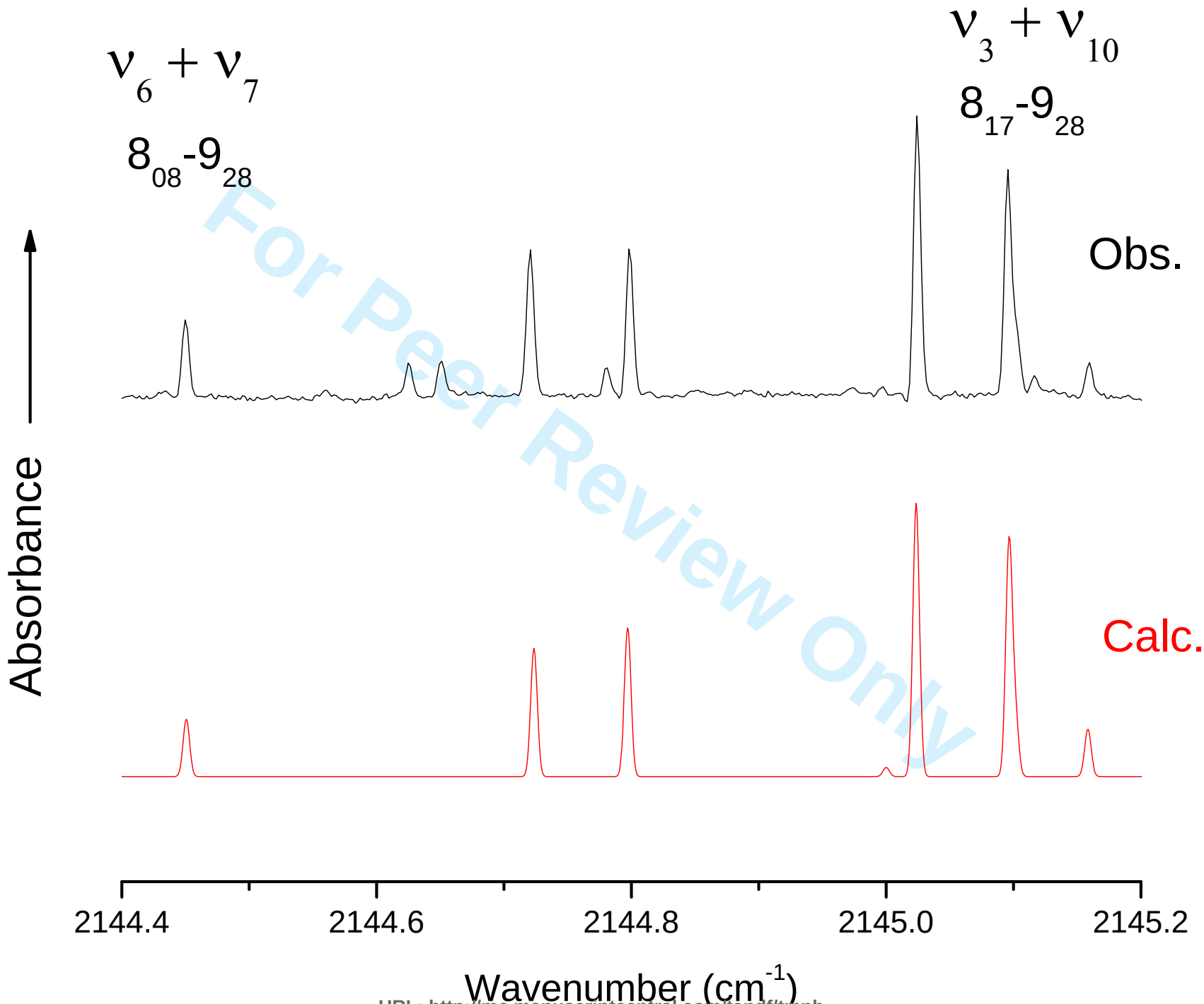

Fig. 5

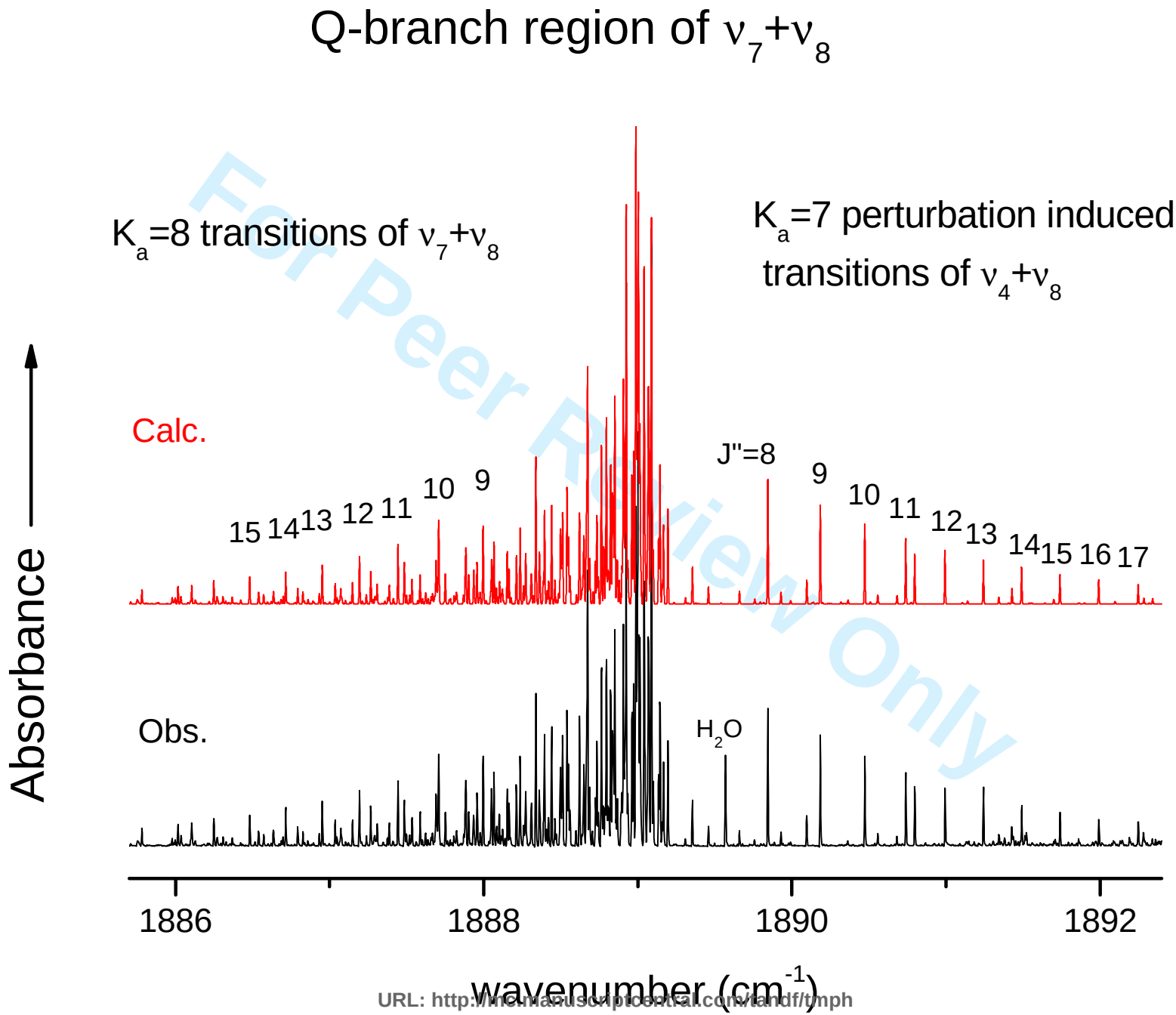

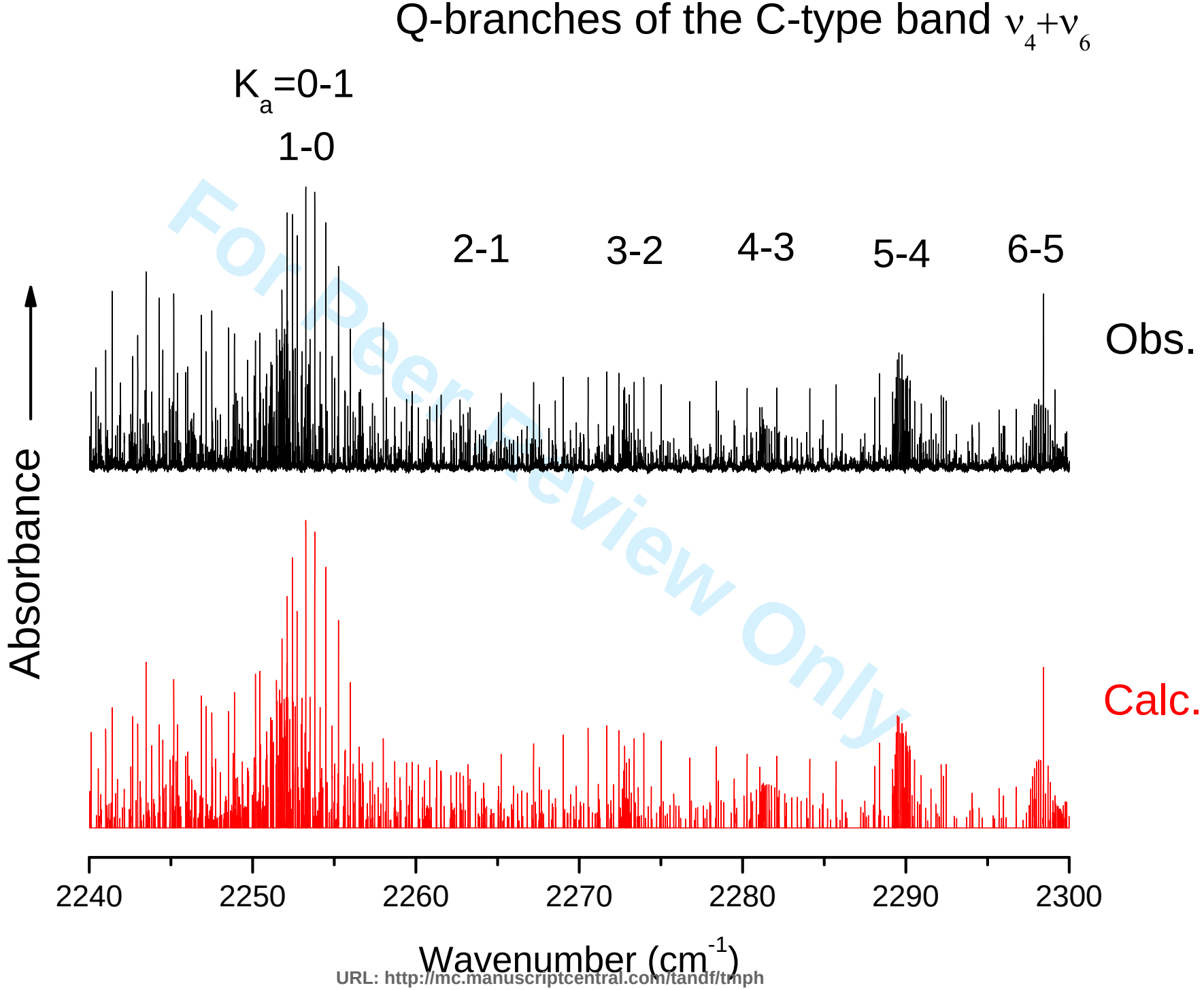

Fig. 7

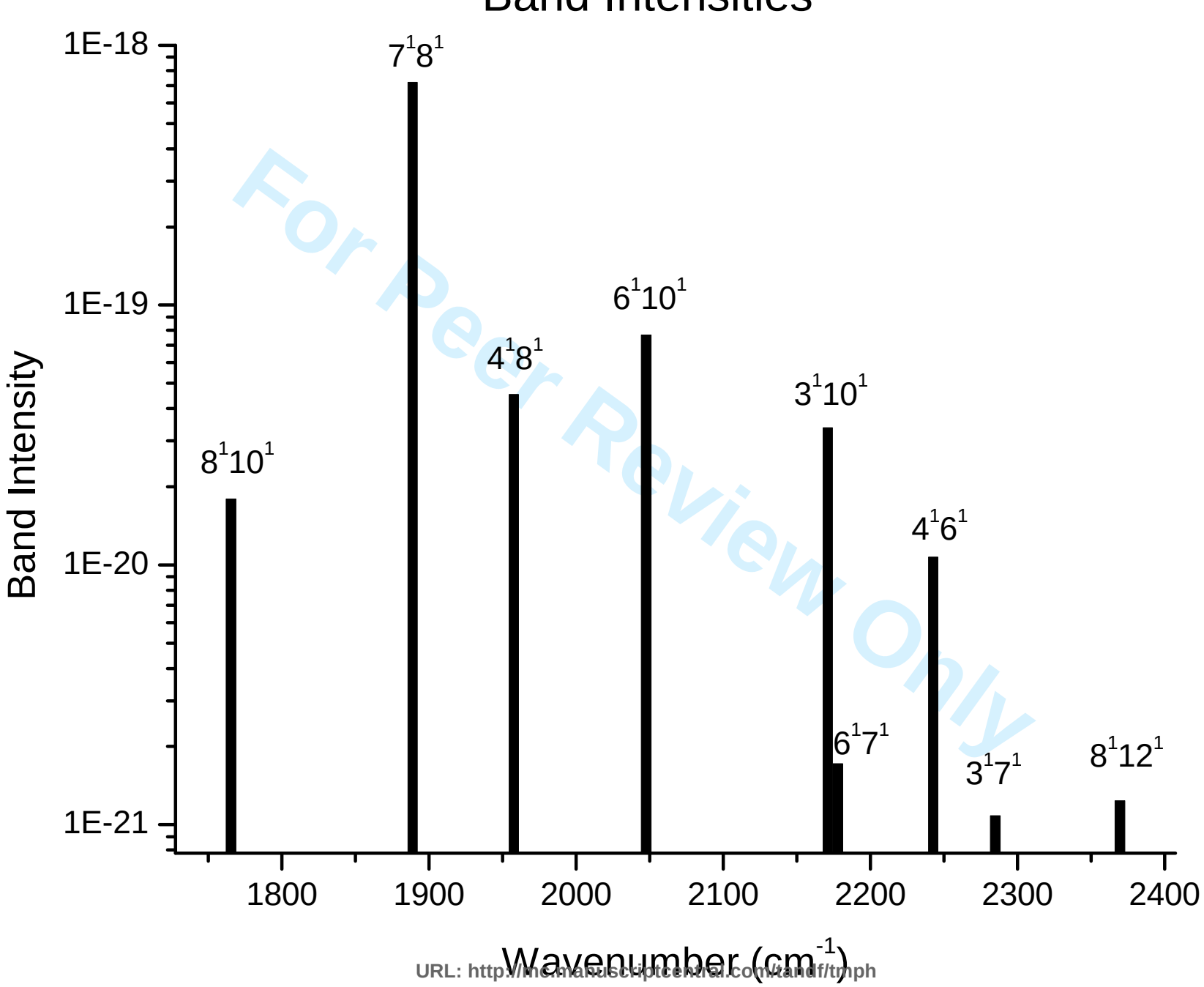

Fig. 8

Table 1. Hamiltonian matrix used to calculate the $\{8^1 10^1, 7^1 8^1, 4^1 8^1, 8^1 12^1, 6^1 10^1, 6^1 7^1, 4^1 6^1, 3^1 10^1, 3^1 7^1\}$ interacting states of ethylene.

Table 2. Range of quantum numbers observed for experimental energy levels of the vibrational states $\{7^1 8^1, 4^1 8^1, 6^1 10^1, 3^1 10^1, 6^1 7^1, 4^1 6^1, 3^1 10^1\}$ of ethylene and statistical analysis of the results.

Table 3. Vibrational band centers, rotational and anharmonic and Coriolis interaction constants (in cm^{-1}) for the ground state and the $\{8^1 10^1, 7^1 8^1, 4^1 8^1, 8^1 12^1, 6^1 10^1, 6^1 7^1, 4^1 6^1, 3^1 10^1, 3^1 7^1\}$ interacting states of ethylene**.**

Footnotes:

[a]Ground state values from ref.[1].

[b]Uncertainties are given in parentheses in units of the last significant digits as stated, in terms of one standard deviation σ in the least squares adjustment.

[c]Fixed at ground state values.

[d]For the sake of clarity, we give here the operator rather than the corresponding constant.

Table 4. Transition moment constants (in Debye) for the $\nu_7 + \nu_8$, $\nu_4 + \nu_8$, $\nu_6 + \nu_{10}$, $\nu_4 + \nu_6$ and $\nu_8 + \nu_{10}$ bands of ethylene.

Footnote:

[a]Uncertainties are given in parentheses in units of the last significant digits as stated, in terms of one standard deviation σ in the least squares adjustment.

Table 1.

	$8^1 10^1$	$7^1\ 8^1$	$4^1 8^1$	$8^1 12^1$	$6^1 10^1$	$6^1 7^1$	$4^1 6^1$	$3^1 10^1$	$3^1 7^1$
$8^1 10^1$	H_W	Herm conj	Herm conj	Herm conj					
$7^1\ 8^1$	C^A	H_W	Herm conj	Herm conj	Herm conj				
$4^1 8^1$	C^B	C^C	H_W	Herm conj	Herm conj				
$8^1 12^1$	C^C	C^B	C^A	H_W			Herm conj		
$6^1 10^1$		F	C^C		H_W	Herm conj	Herm conj	Herm conj	
$6^1 7^1$					C^A	H_W	Herm conj	Herm conj	
$4^1 6^1$				F	C^B	C^C	H_W		
$3^1 10^1$					C^C	C^B		H_W	Herm conj
$3^1 7^1$								C^A	H_W

v-diagonal operators:

$$
\begin{aligned}
&H_W = E_v + \left[A^v - \tfrac{1}{2}\left(B^v + C^v\right)\right] J_z^2 + \tfrac{1}{2}\left(B^v + C^v\right) J^2 + \tfrac{1}{2}\left(B^v - C^v\right) J_{xy}^2 \\
&- \Delta_K^v J_z^4 - \Delta_{JK}^v J_z^2 \mathbf{J}^2 - \Delta_J^v \left(\mathbf{J}^2\right)^2 - \delta_K^v \left\{J_z^2, J_{xy}^2\right\} - 2\delta_J^v J_{xy}^2 \mathbf{J}^2 \\
&+ H_K^v J_z^6 + H_{KJ}^v J_z^4 \mathbf{J}^2 + H_{JK}^v J_z^2 \left(\mathbf{J}^2\right)^2 + H_J^v \left(\mathbf{J}^2\right)^3 \\
&+ h_K^v \left\{J_z^4, J_{xy}^2\right\} + h_{KJ}^v \left\{J_z^2, J_{xy}^2\right\} \mathbf{J}^2 + 2h_J^v J_{xy}^2 \left(\mathbf{J}^2\right)^2 \\
&+ L_K^v J_z^8 + L_{KKJ}^v J_z^6 \mathbf{J}^2 + L_{KJ}^v J_z^4 \left(\mathbf{J}^2\right)^2 + L_{JJK}^v J_z^2 \left(\mathbf{J}^2\right)^3 + L_J^v \left(\mathbf{J}^2\right)^4 \\
&+ l_K^v \left\{J_z^6, J_{xy}^2\right\} + l_{KJ}^v \left\{J_z^4, J_{xy}^2\right\} \mathbf{J}^2 + l_{JK}^v \left\{J_z^2, J_{xy}^2\right\} \left(\mathbf{J}^2\right)^2 + 2l_J^v J_{xy}^2 \left(\mathbf{J}^2\right)^3 \\
&+ P_K^v J_z^{10} + P_{KKKJ}^v J_z^8 \mathbf{J}^2 + P_{KKJ}^v J_z^6 \mathbf{J}^4 + \ldots
\end{aligned}
$$

v-off-diagonal operators:

$$
\begin{aligned}
F &= h_1^F + h_2^F \mathbf{J}^2 + h_3^F J_z^2 + h_4^F J_{xy}^2 + \ldots \\
C^A &= h_1^A J_z + h_2^A \{i J_y, J_x\} + \ldots \\
C^B &= h_1^B J_x + h_2^B \{i J_y, J_z\} + \ldots \\
C^C &= h_1^C i^* J_y + h_2^C \{J_x, J_z\} + \ldots
\end{aligned}
$$

with $\{A, B\} = AB + BA$, $J_\pm = J_x \mp i J_y$ and $J_{xy}^2 = J_x^2 - J_y^2$.

Table 2.

Vibrational State	$7^1 8^1$	$4^1 8^1$	$6^1 10^1$	$6^1 7^1$	$4^1 6^1$	$3^1 10^1$
Number of Levels	569	244	293	16	222	262
J_{max}	35	27	26	21	24	27
K_{max}	13	8	9	6-7	8	12
$0.000 \leq \delta < 0.002$	86.6%	94.3%	89.4%	81.3%	63.8%	84.4%
$0.002 \leq \delta < 0.004$	8.8%	3.3%	7.5%	0.0%	16.3%	9.5%
$0.004 \leq \delta < 0.008$	3.9%	2.4%	3.1%	18.7%	16.3%	5.3%
$0.008 \leq \delta < 0.016$	0.7%				3.6%	0.8%
Std, Deviation (10^{-3} cm^{-1})	2.1					

Table 3.

	0^0	$8^1 10^1$	$7^1 8^1$	$4^1 8^1$	$8^1 12^1$
E_v/hc		1765.603 (31)[b]	1888.9783 (20)[b]	1958.2850 (20)[b]	2369.72 (130)[b]
A	4.86462016[a]	4.789826 (440)	4.70879 (130)	4.68617 (300)	4.875 (140)
B	1.00105650	1.003269 (230)	0.9952615 (460)	0.992108 (120)	1.04244 (820)
C	0.82804599	0.821647 (220)	0.830599661 (860)	0.8302158 (110)	c
$\Delta_K \times 10^4$	0.864798	0.69506 (9900)	0.57329 (3700)	0.23714 (1700)	c
$\Delta_{JK} \times 10^4$	0.1023214	c	c	c	c
$\Delta_J \times 10^5$	0.1470224	c	0.1405264 (1400)	0.233635 (3600)	c
$\delta_K \times 10^4$	0.101590	c	0.23497 (2400)	0.68669 (3600)	c
$\delta_J \times 10^6$	0.281684	c	0.283051 (8900)	0.61546 (4200)	c
$H_K \times 10^8$	0.6196	c	c	c	c
$H_{KJ} \times 10^9$	-0.424	c	c	c	c
$H_{JK} \times 10^9$	0.1845	c	c	c	c
$H_J \times 10^{11}$	0.2501	c	c	c	c
$h_K \times 10^8$	0.346	c	c	c	c
$h_{KJ} \times 10^9$	0.1138	c	c	c	c
$h_J \times 10^{11}$	0.1098	c	c	c	c
	$6^1 10^1$	$6^1 7^1$	$4^1 6^1$	$3^1 10^1$	$3^1 7^1$
E_v/hc	2047.7589 (20)[b]	2178.011 (60)[b]	2252.8026 (24)[b]	2171.2397 (20)[b]	2285.048 (50)[b]
A	4.94859 (210)	5.0754 (250)	4.902101 (240)	4.89652 (320)	4.93033 (300)
B	1.00580 (220)	0.99400 (170)	0.99557 (220)	0.9844828 (710)	0.99517 (450)
C	0.8232976 (140)	0.82334 (200)	0.8244953 (270)	0.8274741 (180)	c
$\Delta_K \times 10^4$	1.3271 (2100)	2.799 (1000)	0.62587 (9500)	0.3000 (1200)	c
$\Delta_{JK} \times 10^4$	-0.27411 (6800)	c	0.78471 (9300)	c	c
$\Delta_J \times 10^5$	0.153455 (8300)	c	0.15844 (1500)	0.07439 (3100)	c
$\delta_K \times 10^4$	c	c	0.22507 (6900)	0.19622 (9400)	c
$\delta_J \times 10^6$	0.33335 (4700)	c	0.33426 (8900)	-0.1496 (1000)	c

Coupling constants[d]

Operator	**<7¹8¹|8¹10¹>**	**<8¹12¹|4¹8¹>**	**<6¹7¹|6¹10¹>**	**<3¹7¹|3¹10¹>**
J_z	-4.47108 (4300)	-3.825 (1600)	-3.6308 (3800)	-4.59692 (3900)
$\{ i J_y , J_x \} \times 10^3$	-7.2682(1900)		-12.2157 (7000)	
$J_z J^2 \times 10^4$	-2.7184 (1300)			
$\{ J_z , J_{xy}^2 \} \times 10^4$	-4.1497 (8000)			
$\left\{ \{ i J_y , J_x \}, J_z^2 \right\} \times 10^6$	6.647 (2500)		46.02 (1200)	
$J_z^3 \times 10^3$				-1.91320 (7200)
Operator	**<4¹8¹|8¹10¹>**	**<8¹12¹|7¹8¹>**	**<4¹6¹|6¹10¹>**	**<3¹10¹|6¹7¹>**
J_x	1.789851(7200)	1.705810(7700)	2.0381(1100)	-0.0012311(4000)
$\{ i J_y , J_z \} \times 10^2$	-4.3918 (1800)		-9.4562(3400)	-3.5923(2300)
$J_x J^2 \times 10^5$				-6.536(2900)
$\{ J_x , J_z^2 \} \times 10^3$				-1.1786(2300)
$(J_-^3 + J_+^3) \times 10^5$	2.2733 (4000)			
Operator	**<4¹8¹|7¹8¹>**	**<4¹6¹|6¹7¹>**	**<3¹10¹|6¹10¹>**	**<6¹10¹|4¹8¹>**
$i J_y$				-0.247161(8600)
$\{ J_x , J_z \} \times 10^2$	-1.3048(2600)	-1.7127(1800)	4.7478(2600)	
$\left\{ \{ J_x , J_z \}, J_z^2 \right\} \times 10^6$	9.938(1900)			
$\{ J_x , J_z \} J^2 \times 10^6$		-4.5131(8300)		

$(J_-^3 - J_+^3)\times 10^5$	-1.6251(1500)	-4.5424(9700)	2.9109(5200)	-2.1243(5300)
$J^2(J_-^3 - J_+^3)\times 10^9$	2.477(1400)			
Operator	**$<6^1 10^1 \vert 7^1 8^1>$**	**$<4^1 6^1 \vert 8^1 12^1>$**		
J^2 x 10^3	-6.0037(4700)			
$J_{xy}^2 \times 10^3$	-2.0718(3100)			
$\{J_z^2, J_{xy}^2\}\times 10^5$		9.743(1900)		

Table 4.

Operator	$\nu_7 + \nu_8$	$\nu_4 + \nu_8$	$\nu_6 + \nu_{10}$	$\nu_4 + \nu_6$	$\nu_6 + \nu_{10}$
φ_z x 10^{-1}	0.6365(30)[a]		0.2106(10)		
½({ φ_x ,iJ_y}-{i φ_y,J_x})			0.6771(970) x 10^{-4}		
{φ_z.J_z^2}			-0.2407(450) x 10^{-4}		
φ_x x 10^{-1}		-0.123215(80)			0.129605(90)
{$i\varphi_y$,J_z}		0.1533(120) x 10^{-3}			-0.1424(260) x 10^{-3}
{φ_z,iJ_y}		-0.4350(400) x 10^{-4}			0.4752(510) x 10^{-4}
$i\varphi_y$ x 10^{-2}				0.6945(60)	
{φ_x,J_z}				0.813(110) x 10^{-4}	